Ultra-thin flame retardant polymer nanocomposite coating based on synergistic effect of graphene and glass sheets

Kangtai Ou[1, 3], Zheming Liu[1], Zixuan Liu[1], Qiang Fu[1,2*], Yang Cao[1], Qichao Liu[1], Youyi Sun[1, 3*]

1.School of materials science and technology, North University of China, Taiyuan 030051, P.R. China.

2.School of Civil and Environmental Engineering, University of Technology Sydney, Ultimo NSW 2007, Australia.

3. Changzhou Polyolefin New Material Technology Co., Ltd, Changzhou 213149, P.R. China.

Abstract: It is still a high challenge to develop environmental-friendly and highly efficient flame retardant for application in thin polymer coating. Here, a graphene@glass sheets composite flame retardant is developed and prepared by a new in-situ liquid-phase exfoliation process. When the flame retardant is doped into polymer coating, it exhibits excellent flame retardancy for flammable plastic, wood and nonflammable steel. The limiting oxygen index (ca.32.3%) and UL-94 V-0 rating of a ultra-thin polymer coating (ca.65um) can be obtained for fire protection of wood. The long fire-retardant time (55.0min) is also observed, which is far longer than that of the conventional polymer coating (1.0min) for fire protection of steel. This work provides a new strategy for creating cost-effective thin flame retardant polymer coatings for various industrial applications.

Keywords: Glass sheets, graphene, in-situ synthesis, flame retardant, thin fireproof polymer coating

---

Responding author: Fax: 86-351-3559669

E-mail address: syyi@pku.edu.cn (YY Sun); qiang.fu@uts.edu.au (QF).

1.Introduction

With the rapid development of the world economy, there are more and more plastic, wood and steel in the whole industry[1-2]. However, the flammable plastic and wood to nonflammable steel bring huge potential safety hazards for the industry, especially construction field[1, 3]. The flame retardant polymer coating is a good strategy for fire protection of plastic, wood and steel[4-5]. As well-known, the performance of flame retardant polymer coating mainly depends on chemical structure and composition of flame retardant [6-9]. Therefore, a lots of flame retardants have been developed for application in flame retardant polymer coating, such as halogen system, phosphorus nitrogen system, intumescent system, biomass system, carbon system, 2D MXenes and so on [10-21]. Among these flame retardants, carbon (eg. Graphene) system is a promising flame retardant due to good environmental friendly and good mechanical reinforcement[22]. However, it showed relatively low flame retardancy for the single graphene materials. So, graphene based composite flame retardants were developed for improving flame retardancy[23-24]. For example, phosphor nitrile functionalized UiO-66-NH_2@graphene hybrid flame retardants were prepared for fire safety of epoxy [25]. Graphene nanosheets decorated by cerium stannate were also prepared to enhance flame retardancy and mechanical performances of flexible polyurethane foam [26]. The $Mg(OH)_2$@graphene oxide (MHG) nanocomposite was prepared by a facile precipitation method for fire safety of PVA[27]. However, the graphene system was few applied in flame retardant polymer coating due to following several reasons. Firstly, the char of these flame retardant-doped polymer coating was not stable enough to form defence and thick film against fire [28]. Secondly, the incompatibility between flame retardant and polymer matrix further limited the processability and flame retardancy of such flame retardant polymer coating [29]. Therefore, it is still an ambitious challenge to develop flame retardant polymer coating with high performance, especially for graphene based flame retardants.

Based on above consideration, a new biomimetic low-melting glass sheets (GPs)@graphene nanosheets(GNs)@Poly(Hydroxyethyl acrylate-co-Sodium vinyl sulfonate) (PVH) flame retardant is designed and prepare by in-situ aqueous exfoliation

method. The GPs are flowable and noncombustible at high temperature, which act as synergism to enhance the flame retardancy of graphene. In addition, PVH acts as surfactant for improving compatibility between GPs@GNs and polymer matrix. So, it also exhibits high mechanical stability and flame retardancy for present flame retardant polymer coating. This work offers a new approach to large-scale produce low-cost and effective flame retardant coatings, which hold great promise for many real-world applications in construction, transportation, plumbing, and electrical fields.

2. Experiment

2.1 Materials

Hydroxyethyl acrylate (HEA), sodium vinyl sulfonate solution (SVS, 25wt%) , potassium persulfate and graphite were supplied by Aladdin Chemical Co., Ltd. The low-melting glass powders (GPs) was supplied by Aladdin Chemical Co., Ltd. H_2SO_4 (≥98.0%) was purchased from Chengdu Ke Long Chemical Reagent Co., Ltd. H_3PO_4, NaOH and Na_2CO_3 were purchased from Tianjin Damao technology development Co., Ltd. Waterborne acrylic acid resin paint (AA, 50±2wt%) was supplied by Zhejiang Jinhong adhesive Co., Ltd.

2.2 Preparation of GPs@GNs@PVH flame retardant

The GPs@GNs@PVH flame retardant was prepared by a facile three-step method as shown in following. Firstly, the PVH was synthesized by the aqueous solution polymerization method according to previous work[30]. The 130.0g SVS aqueous solution, 20.0g HEA and 25.0g water were added to 250.0mL three-mouth flask and mixed by mechanical stirring for 3.0min. 61.0g potassium persulfate aqueous solution (0.9wt%) was dropped into above solution for 1.0h and continuously reacted for 5.0h at 65.0℃ under mechanical stirring. Finally, 0.065g potassium persulfate powder was directly added to above reaction solution and continuously reacted for 1h at 65.0℃ under mechanical stirring, forming PVH solution (30.0wt%). Secondly, the expanded graphite (EG) was prepared by bubbling expansion method. 30.0g $KMnO_4$ was added into 180.0mL concentrated sulfuric acid in the ice bath. 30.0g natural graphite was added to above solution and mechanically stirred at room temperature for 1.0h. Then, 30.0g Na_2CO_3 was added into above mixture under mechanical stirring. Secondly, 420.0mL H_3PO_4 was added into above mixed system under mechanical stirring for 5.0h. Thereafter, the products were washed and filtered, forming EG. Thirdly, 96.0g EG, 260.0g GPs and 87.0mL PVH solution were added into 818.0mL NaOH solution (pH=14). The mixture was mechanically stirred for 2.0h at 15,000 rpm by using an FA

40 high shear dispersing emulsifier (Fluko), forming GPs@GNs@PVH dispersion solution (31.8wt%). In a comparison, the GPs@GNs dispersion solution (30.0wt%) was also prepared by the similar process.

2.3 Preparation of flame retardant AA coating

The flame retardant AA coating was prepared by the facile mixing method. The 500.0g GPs@GNs@PVH (or GPs@G) dispersion solution and 600.0g waterborne AA paint were mixed under mechanical stirring (1000r/min) for 30.0min to obtain uniform flame retardant paint. The composition of flame retardant paint is shown in Table 1. After that, the paint was coated on the surface of various substrates (eg. PMMA plate, PU foam, wood and steel) by spraying method and cured at room temperature for 24.0h, forming flame retardant AA coating.

Table 1. The composition of various flame retardant paints

Sample	AA (wt%)	SiO_2 (wt%)	GPs (wt%)	G (wt%)	PVH (wt%)	Other reagent (wt%)
GPs@GNs@PVH/ AA	17.0	10.0	9.8	3.6	1.0	0.3
GPs@GNs/AA	17.0	10.0	9.8	3.6	0	0.3

2.4 Characterization

The phase structure of the samples was characterized by the X-ray diffraction (XRD) with a Cu K_α radiation diffraction (λ=0.154nm, 35.0kV and 40.0mA) in the scan range of 5.0~80.0° and the scanning speed of 4.0°/min.

Raman spectra were obtained by a Renishaw in Via Raman microscope with a 532.0nm laser wavelength.

The thickness of the graphene nanosheets was obtained by atomic force microscopy (AFM, SPA-300HV, SII).

Fourier transform infrared spectroscopy (FT-IR) spectrum was obtained by an infrared spectrometer (TENSOR 27, Bruker, Germany).

Thermal properties of coatings were characterized by thermogravimetric analysis (TGA, Mettler Toledo, Switzerland, 20℃/min, 25~800℃).

The melt transition behavior of GPs was characterized by Image burning point tester (CJY-1400) according to QB/T 1546-2016.

The micro-structure of sample was observed by Field emission scanning electron microscopy (SEM, Su-8010).

The thickness of coating on wood and PU foam was obtained by observing their sectional structure with a metallographic microscope (MV6100), and the thickness of coating on steel sheet was measured with a digital display screw micrometer (IP64).

The adhesive performance of flame retardant AA coating on PMMA and steel was characterized by knife-scratch and shear-lap tests according to ASTM D 3359-09 and ISO 4587, respectively.

The adhesive performance of flame retardant AA coating on PMMA was also characterized by adhesive strength as shown in Scheme 1. The testing sample was stretched by stretching machine with a rate of 20.0mm/min. The shearing strength (MPa) of testing sample is calculated according to following formula (1).

$$\text{Shearing strength}=F/S \qquad (1)$$

Where F and S is the tensile force (N) and coating area (mm^2), respectively.

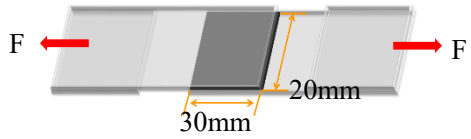

Scheme 1. Schematic of testing adhesive strength.

2.5 Flame retardancy of flame retardant AA coating

Limited oxygen index (LOI) of flame retardant AA coating was measured by an oxygen index meter (JF-3, Nanjing Jiangning Analytical Instrument, China).

UL-94 rating of flame retardant AA coating was measured by a horizontal vertical burning meter (CZF-3, Nanjing Jiangning Analytical Instrument, China) according to GB4609-84 standards.

The flame retardancy was evaluated for plastic, wood and steel as shown in following. A Bunsen lamp filled with butane gas was used as the fire source in the experiment. The distance between the flame and the coating was adjusted to 7.0cm. The combustion process was recorded by camera.

The thermal insulation performance and fire resistance time of the flame retardant AA coating were tested by large plate experiment on the basis of ASTM E119 standards as shown in Scheme 2. During this process, the coated side of the steel plate was exposed to a high temperature flame (about 1000℃), and the back side temperature of the steel plate was recorded as a function of time by the Infrared Thermal Imager. Fire-resistant time is defined as the time for the back side temperature of the steel plate to reach 200℃ from room temperature, which is regarded as a standard of evaluating fire resistance of the flame retardant coatings.

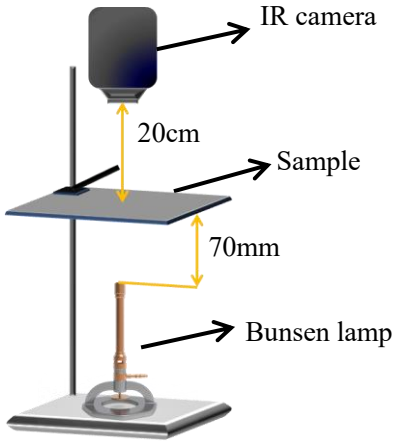

Scheme 2. Schematic of testing fire resistance time.

3. Results and Discussions

Generally, the graphene based flame retardants were prepared by a two-step method[31-32]. The graphene nanosheets (GNs) or reduced graphene oxide (rGO) was firstly prepared by chemical or physical method. And then, other flame retardants were combined with GNs or rGO by in-situ synthesis or directly mixing method. As well-known, the GNs or rGO easily formed agglomeration in the preparing process, and the GPs also easily precipitated in water due to large density. The two problems bring a difficult and challenge for preparing GPs@GNs flame retardant with uniform distribution[33]. Here, a new preparing process was developed to produce GPs@GNs flame retardant, which was prepared by in-situ water-phase exfoliation under assistant of bubbling expansion as shown in Fig.1. Some oxygen groups were firstly introduced to the edges of graphite flakes by chemical treatment, and then the layer spacing of graphite flakes was expanded by gas bubbles (Video 1). Above process was used to minimize the attractive interaction between graphite layers. So, the pre-treated graphite flakes were easily exfoliated to GNs by high-rate shearing force in presence of GPs and PVH, forming GPs@GNs@PVH flame retardant with homophonous distribution. The successful preparation of GPs@GNs@PVH flame retardant facilitates the industrial application of graphene based flame retardant.

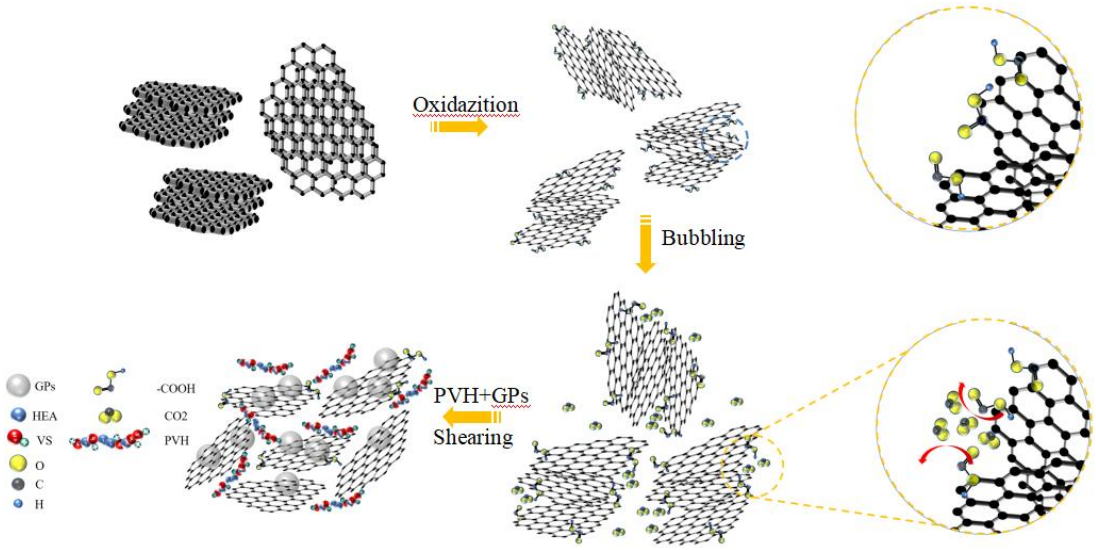

Fig.1. Schematic illustration of the synthesis processes of GPs@GNs@PVH flame retardant.

The formation of GPs@GNs@PVH was confirmed by XRD, Raman and IR spectrum as shown in Fig.2A, 2B and 2C, respectively. A strong diffraction peak of 2θ=26.5° was observed (in Fig.2A-a), which was assigned to (002) pattern of graphite. After chemical treatment and exfoliation process, the diffraction peak of 26.5° almost disappeared (Fig.2A-b/c). This result indicated that the graphite flaks with order crystal structure changed to graphene nanosheets with disorder structure due to the mechanical exfoliation[34]. Other diffraction peaks were assigned to GPs. As shown in Fig.2B, two strong peaks at 1351.0cm^{-1} and 1584.0cm^{-1} were clearly observed for GPs@GNs and GPs@GNs@PVH, which were assigned to D and G band of graphene, respectively. The D to G intensity ratio (I_D/I_G) of GPs@GNs@PVH and GPs@GNs was about 0.3 and 0.6, respectively. The result indicated that some defects (eg. oxide groups) were introduced into the surface of GNs after chemical treatment. In addition, it was found that the I_D/I_G of present graphene based composites was obviously smaller than that of other graphene based composites reported in previous works [35-36]. As shown in Fig.2C-a, there was almost no absorption peaks for the GPs@GNs. In a comparison, some absorption peaks were clearly observed for the GPs@GNs@PVH (Fig.2C-b), which were similar with IR spectrum of pure PVH (Fig.2C-c). The result indicated that these new absorption peaks were assigned to PVH. These results confirm the formation of GPs@GNs@PVH by in-situ water-phase exfoliation.

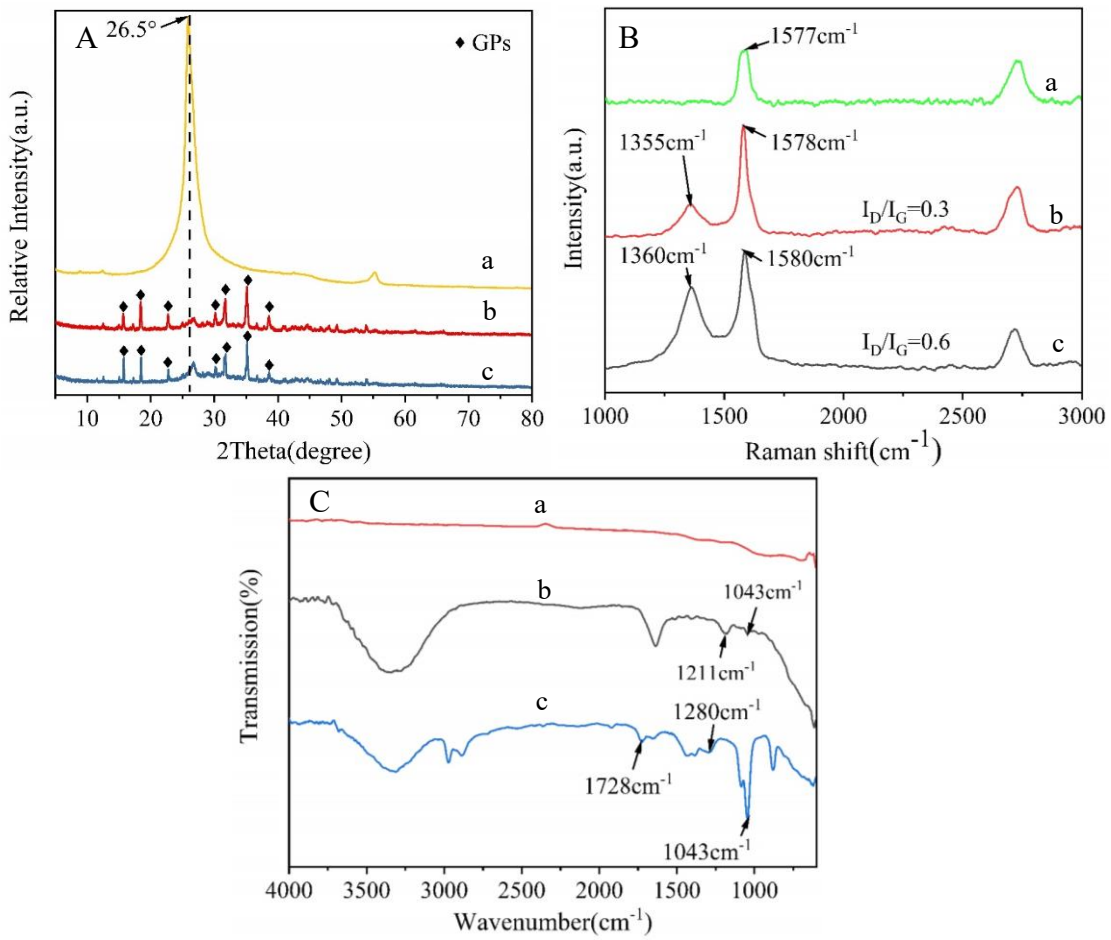

Fig.2. (A) XRD and (B) Raman spectra of (a) graphite, (b) GPs@GNs@PVH and (c) GPs@GNs. (C) IR spectra of (a) GPs@GNs, (b) GPs@GNs@PVH and (c) pure PVH

The micro-structure of GPs@GNs@PVH was characterized by the SEM images as shown in Fig.3A. The GPs@GNs@PVH exhibited a typical flake shape with a size of ca.2.5um. The special flake shape of present composites was assigned to flake shape of GPs and GNs (sFig.1A). In addition, the EDS mapping images of GPs were further characterized as shown in sFig.1B. The Si, O and Na element were clearly observed, indicating that the GPs with low melting point were mainly composed of Si, O and Na element. From the high magnification SEM (Fig.3B), some nanosheets were observed, which were assigned to graphene. The result indicated that GPs were flake and wrapped by GNs. Above result was further confirmed by element mapping image (Fig.3D-a-d). Expecting for Si, O and Na element, a new C element was clearly observed, which was assigned to graphene and PVH. In addition, these elements were uniformly distributed on the surface of particles. The result further indicated that these flakes were

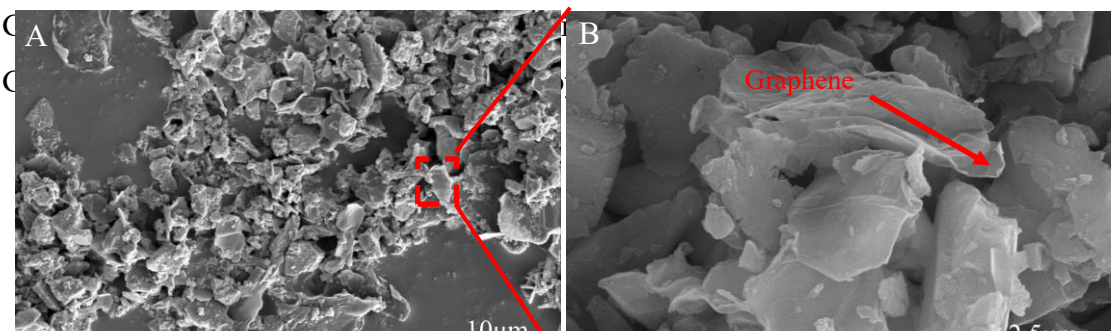

some sheets with a thickness of *ca.* 1.1nm, forming single- or two-layer(s) graphene. The result further confirmed that the EG was in-situ exfoliation to GNs with ultra-thin layer(s) in the presence of GPs. The GPs@GNs@PVH dispersion solution showed clear and transparent after centrifugation (3000rpm) as shown in Fig.3E. The GNs generally were stable in water under centrifugation (3000rpm), revealing a black dispersion solution. The result further indicated that the GNs were coated on surface of GPs. The GPs@GNs@PVH dispersion aqueous solution remained good stability for more than 24.0h (Fig.3D-d). In contrast, the GPs@GNs was complete precipitation from GPs@GNs dispersion aqueous solution within 24.0h. These results confirmed that the PVH could provide good stability and dispersion of GPs@GNs in aqueous solution.

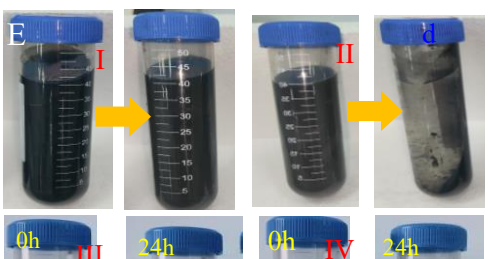

Fig.3. (A-B) SEM images of GPs@GNs@PVH, (C) AFM image of graphene in GPs@GNs@PVH. (D) The element mapping images of GPs@GNs@PVH, (a) Si, (b) C, (c) Na and (d) O. (E) Optical photos of (I) graphene and (II) GPs@GNs@PVH dispersion solution before and after centrifugation, (III) GPs@GNs and (IV) GPs@GNs@PVH dispersion solution after 24.0h.

To evaluate application of GPs@GNs@PVH flame retardant in industries, one type of commercial waterborne acrylic resin (AA) paint was chose as the matrix of flame retardant polymer coating. The micro-structure of flame retardant AA coating with GPs@GNs and GPs@GNs@PVH was characterized and compared by SEM images as shown in Fig.4. It clearly showed a relative smooth surface and few large particles was observed for the pure AA coating (Fig.4A). When the GPs@GNs was doped into AA coating, it presented lots of large particles and pores (Fig.4B). The result indicated poor interface interaction between GPs@GNs fillers and AA matrix. In contrast, it exhibited a relatively few pore and a lots of embedding particles for GPs@GNs@PVH/AA coating (Fig.4C). The result indicated the strong interfacial interaction between GPs@GNs@PVH and AA matrix, which was mainly ascribed to the PVH. At the same reason, there was few aggregates for the flame retardant. AA coating, indicating the good distribution of GPs@GNs@PVH in AA matrix. Such robust interfacial property and good distribution could effectively improve flame retardancy, thermal and mechanical properties of flame retardant AA coating. Fig.4D shows the Raman spectra of flame retardant AA coating with GPs@GNs and GPs@GNs@PVH. It clearly showed two strong peaks at 1352.0 (or 1362.0) cm^{-1} and 1587.0cm^{-1}, which were assigned to D and G band of graphene, respectively[37]. Although these GNs were not clearly observed in SEM images due to coat on surface of GPs, yet, the Raman result could confirm the presence of GNs in flame retardant AA coating.

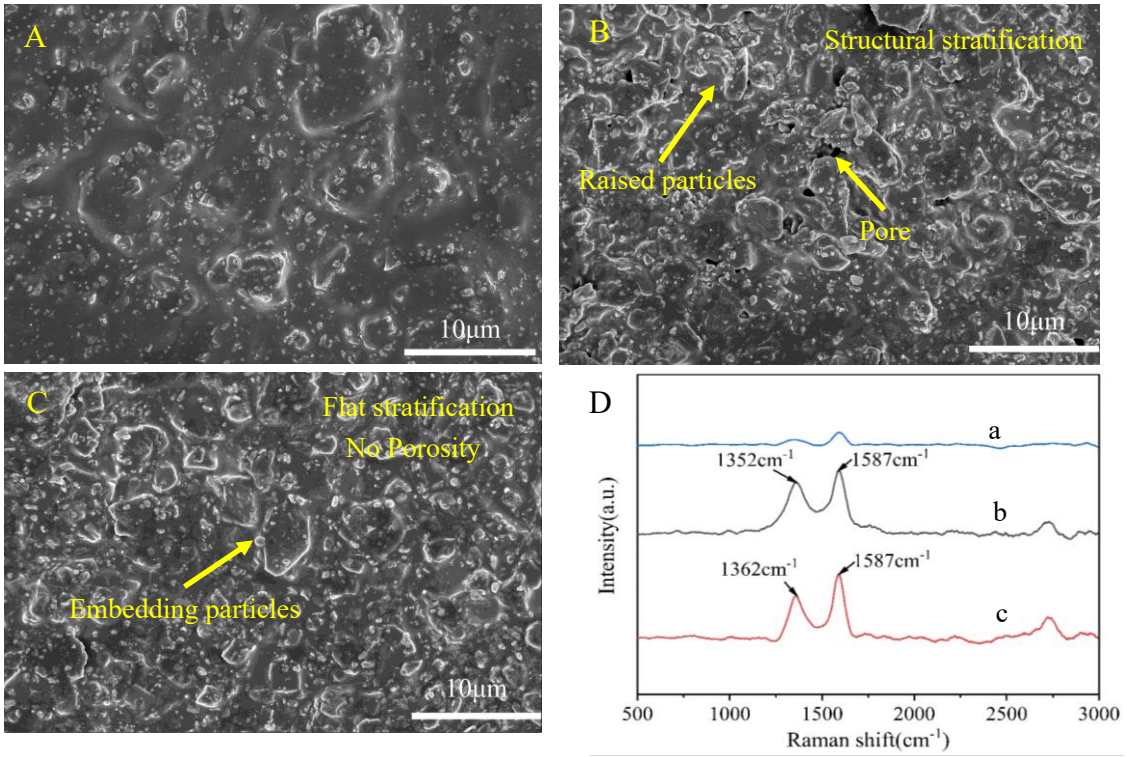

Fig.4. SEM images of (A) AA coating, (B) GPs@GNs/AA coating and (C) GPs@GNs@PVH/AA coating. (D)Raman spectra of (a) AA coating, (b) GPs@GNs/AA coating and (c) GPs@GNs@PVH/AA coating.

As-well known, the adhesive properties of flame retardant polymer coating on substrate was also key role for its practical applications[38]. Here, the adhesive properties of flame retardant AA coating on PMMA and steel plate were characterized by knife-scratch and shear-lap tests according to ASTM D 3359-09 and ISO 4587 , respectively as shown in Fig.5[39]. Generally, adhesive failures were classified into three modes: cohesive failure, adhesive failure, mixed cohesive and adhesive failure[40]. The cohesive mode corresponded to a failure in the bulk adhesive layer, while the adhesive mode corresponded to the interfacial failure between the adhesive and adherent[41]. The cohesive mode indicated the better adhesive performance comparing to adhesive mode[41]. As shown in Fig.5A, the AA coating exhibited the mixed failure mode, indicating a low adhesive performance. After introduction of GPs@GNs or GPs@GNs@PVH, the flame retardant AA coating exhibited a cohesive failure mode, indicating a good adhesive performance. The adhesive strength of various coatings on PMMA plate was further characterized and compared as shown in Fig.5B. It was about 0.08MPa, 0.58MPa and 0.59MPa for pure AA coating, GPs@GNs/AA coating and GPs@GNs@PVH/AA coating, respectively. The improvement of adhesion strength and toughness was attributed to the presence of reinforcing phase (GPs and

GNs). In addition, the knife-scratch method was also performed to evaluate the adhesion of flame retardant AA coating with the steel substrate as shown in Fig.5C. According to ASTM D3359, it ranged from 0B (complete removal of coating film lattices) to 5B (intact lattices with completely smooth edges)[42]. As shown in Fig.5C, the intact lattices of all coatings exhibited completely smooth edges, indicating the highest adhesion level of 5B. The result further confirmed good adhesive performance of flame retardant AA coating for various substrates.

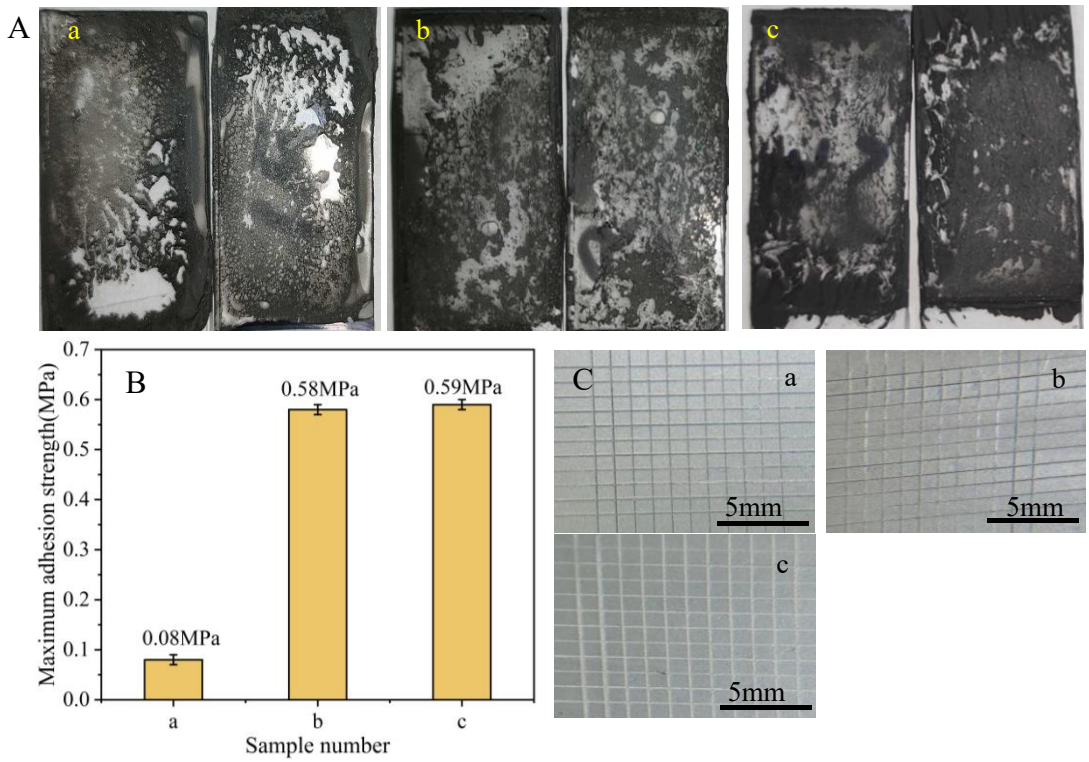

Fig.5. (A)Optical photos of (a) AA coating, (b) GPs@GNs/AA coating and (c) GPs@GNs@PVH/AA coating on PMMA plate after failure. (B) Adhesion strength of (a) AA coating, (b) GPs@GNs/AA coating and (c) GPs@GNs@PVH/AA coating on PMMA plate. (C) Optical photographs of (a) AA coating, (b) GPs@GNs/AA coating and (c) GPs@GNs@PVH/AA coating on metal plate after knife-scratch.

The thermal degradation behavior of various AA coatings was determined by TG-DTG curves under N_2 atmosphere as shown in Fig.6. And the relevant parameters were summarized in Table 2. It was clearly seen that the thermal degradation of all coatings was mainly composed of two stages. The slight weight loss between 100℃ and 200.0℃ was attributed to the evaporation of water, while the loss in the range of 300.0-450.0℃ was related to decomposition of the organic component and resin matrix[43]. For the pure AA coating, the initial decomposition temperature ($T_{5\%}$) and the residual char were

about 210.0℃ and 43.0% (800.0℃), respectively. After addition of GPs@GNs and GPs@GNs@PVH, the $T_{5\%}$ and residual char both increased to ca. 306.0℃ and 62.5% (or 64.3%) , respectively. The higher $T_{5\%}$ of flame retardant AA coatings was due to good barrier effects of GPs@GNs. The remarkably enhancing residual char was also attributed to GPs@GNs, which was difficult to decompose at lower temperature than 800.0℃ under N_2. Here, GPs@GNs/AA coating and GPs@GNs@PVH/AA coating exhibited similar $T_{5\%}$ and residual char. The result was due to that the low content of PVH was slight effect on thermal degradation behavior of coating. The thermal degradation behavior of various AA coatings was also characterized by TG-DTG curves under air atmosphere as shown in sFig.2 and sTable 1. It showed similar result with TG-DTG curves under N_2. The similar residual char indicated the good flame retardancy for present coating [44]. These results suggested that the GPs@GNs or GPs@GNs@PVH could effectively improve thermal stability and residual char of AA coating.

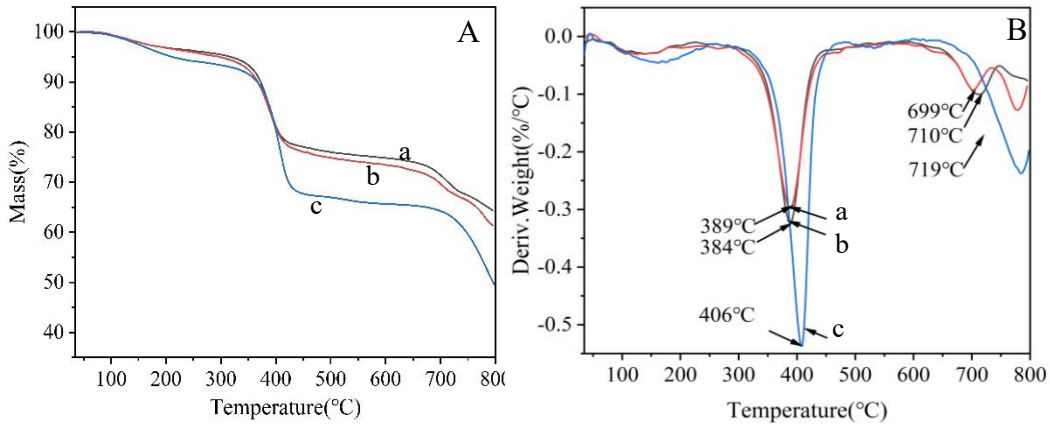

Fig.6. (A) TG and (B) DTA of (a) GPs@GNs/AA coating and (b) GPs@GNs@PVH/AA coating, (c) pure AA coating.

Table 2. The thermal performance of various coatings under N_2.

Coating	$T_{5\%}$ (℃)	T_{max} (℃)	Reidual char (%)
Pure AA	210.0	406.0	49.5
GPs@GNs/AA	306.0	384.0	64.3
GPs@GNs@PVH/AA	306.0	389.0	62.5

The flame retardancy of flame retardant AA coatings was firstly characterized by protection of flammable PMMA plastic as shown in Fig.7. When the pure PMMA plate was exposed to flame for 10.0s, the PMMA plate was ignited and rapidly burnt out within 120.0s (Fig.7A and Video 2). The PMMA plate with AA coating was still be

ignited after exposure to flame for 10.0s, but they burnt more slowly comparing to pure PMMA plate (Fig.7B and Video 3). The result was attributed to that the AA coating contained some inorganic particles (eg. SiO_2) with flame retardancy. In contrast, the flame was not ignited the PMMA plate with GPs@GNs/AA coating and GPs@GNs@PVH/AA coating within 10.0s. In addition, the PMMA plates with flame retardant AA coating almost retained its original integral structure and was few thermal shrinkage deformation (Video 4-5). These results indicated the excellent flame retardancy of present flame retardant AA coatings for plastic materials. The flame retardancy of present flame retardant AA coatings was further evaluated for protection of PU foam (sFig.3). When pure PU foam was exposed to butane flame (>1000.0°C), the PU foam was readily ignited in 3.0s and the most part of PU foam was burnt out within 42.0s (sFig.3A). The PU foam with AA coating or GPs@GNs/AA coating could still be ignited after exposure to flame for 30.0s, but they burnt more slowly comparing to pure PU foam (sFig.3B-C). The burning continued until 98.0s and 47.0s for PU foam with AA coating and GPs@GNs/AA coating, respectively. In a comparison, the PU foam with GPs@G/AA coating had more residual foam comparing to pure PU foam and PU foam with AA coating. In contrast, the PU foam with GPs@GNs@PVH/AA coating had very small flame after exposure to flame for 30.0s. Furthermore, After only 6.0s, the flame was self-extinguishment (sFig.3D). These results further indicated a positive combination or superposition effect between PVH, GNs and GPs, thus leading to better flame retardancy for polymer materials.

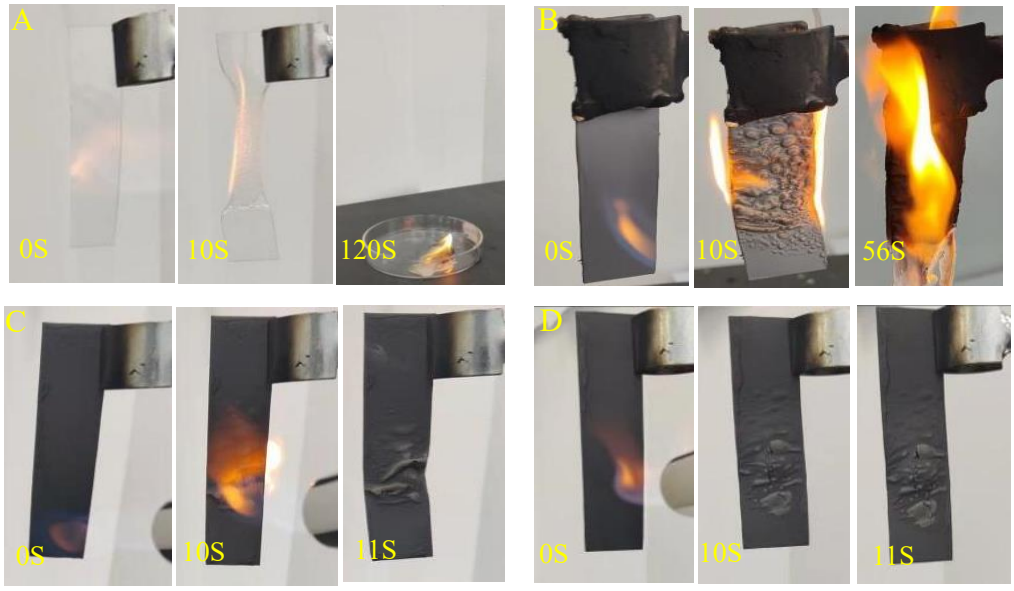

Fig.7. Optical photos of (A) pure PMMA plate, PMMA plate with (B) pure AA coating,

(C)GPs@GNs/AA coating and (D)GPs@GNs@PVH/AA coating in the presence of flame.

The flame retardancy of various AA coatings was evaluated and compared by UL-94 vertical burning and LOI tests as shown in Table 3. Pure PU foam showed a low LOI of ca.19.1% and no UL-94 ratings, agreeing well with previous report[45]. During vertical burning test, upon exposure to flame, PU foam was ignited instantly (<1.0s) until burnt out, leaving a very thin and hollow char after testing. When the PU foam was coated with AA coating, GPs@GNs/AA coating and GPs@GNs@PVH/AA coating (thickness of 500.0um), the LOI was about 21.1%, 26.7% and 31.3%, respectively. When the thickness of GPs@GNs@PVH/AA coating was improved to 600.0um, the LOI of coated PU foam was further improved to be 34.2%. Furthermore, the PU foam with GPs@GNs@PVH/AA coating was self-extinguish within 2.0s after each flame application (sFig.4). However, it still failed to pass a desired UL-94 V-0 rating. This result was due to that the flame retardant AA coating was difficult to form compact protect layer on PU foam with porous structure by the spray method. Above result was further confirmed by testing fire safety of wood without porous structure. When the wood was protected by the GPs@GNs@PVH/AA coating (thickness of ca.65.0um), the LOI could reach 32.3% (Table 3). At the same time, it also exhibited UL-94 V-0 rating for the wood with present flame retardant AA coating. The flame retardancy of present and previous flame retardant polymer coating was also compared for fire safety of wood as shown in Table 3. Present flame retardant AA coating exhibited largest LOI. If the thickness of flame retardant polymer coating was also considered, present flame retardant AA coating indicated better flame retardancy. Here, similar GPs@BN@PVH/AA coating was also prepared and compared, in which the GPs@boron nitride (BN)@PVH had been reported in previous work[46]. The flame retardancy of present GPs@GNs@PVH/AA coating was obvious better comparing to GPs@BN@PVH/AA coating. The result was attributed to following two reasons. Firstly, the surface area of GNs was larger than BN, indicating better barrier effects at the same content. Secondly, the GNs was better dispersion and mechanical reinforcement effect comparing to BN. These results further confirmed the excellent flame retardancy of present GPs@GNs@PVH.

Table 3. Limiting oxygen index (LOI) and dripping behavior of various coatings on PU foam and wood.

Coating	Substrate	Thickness (μm)	LOI (%)	Vertical burning test	Ref
GPs@GNs@PVH/AA	PU foam	500.0	31.3	NR	Present work
GPs@GNs/AA	PU foam	500.0	26.7	NR	
AA	PU foam	500.0	21.1	NR	
GPs@GNs@PVH/AA	PU foam	650.0	34.2	NR	
GPs@GNs@PVH/AA	Wood	65.0	32.3	V-0	
GPs@BN@PVH/AA	Wood	65.0	28.8	NR	
GPs@GNs/AA	Wood	65.0	27.8	V-0	
AA	Wood	65.0	24.6	NR	
Polyphosphate@Montmorillonite/EP	Wood	3000.0	31.8	V-0	[47]
Nitrogen-phosphorus/ EP	Wood	450.0	31.0	V-1	[48]
P@monoacrylate/EP	Wood	100.0	24.0	V-0	[49]
Diethyl bis(2-hydroxyethyl) aminomethylphosphonate/AA	Wood	500.0	28.9	V-0	[50]
bis(4-formyl-2-methoxyphenyl)phenylphosphonate/EP	Wood	200.0	32.9	V-0	[51]

As well-known, the mechanical strength of steel deceased with increasing in temperature, so, it was very important to delay the rise of temperature upon exposure to flame. Present flame retardant AA coating was also evaluated for fire safety of steel plate as shown in Fig.8. When the steel plate with AA coating was exposed to flame, the back side temperature (BT) of the coated steel plate quickly rose from room temperature to more than 261.0℃ within 1.0min (Fig.8C). The result indicated that the fire-resistant time of AA coating was so shorter than 1.0min. In addition, the AA coating was ignited and intense combustion. In contrast, it needed 20.0min and 55.0min to rise to 200.0℃ for BT of the steel plate with GPs@GNs/AA coating and GPs@GNs@PVH/AA coating, respectively (Fig.8D). These results confirmed that Present flame retardant AA coating could effectively reduce heat transfer rate and prolong the fire-resistant time of metal. Furthermore, the GPs@GNs/AA coating and GPs@GNs@PVH/AA coating were not ignited within 55.0min under a flame with a high temperature of ca.1000.0℃ (Fig.8A-B). The result further confirmed excellent

flame retardancy of present flame retardant AA coating. In addition, the wood was one of the most flammable materials, so, the effective fire protection of wood was also high interesting for the industry, buildings, furniture and so on. The fire-resistant of present flame retardant AA coating was further characterized and compared for fire safety of wood as shown in sFig.5. When pure wood was exposure to a alcohol burner flame, it was readily ignited in 1.0s (sFig.5A), indicating a flammability characteristic. In contrast, the wood with GPs@GNs/AA coating and GPs@GNs@PVH/AA coating was still not ignited after exposure to a alcohol burner flame for 80.0min, indicating a long fire-resistant time (sFig.5B-C). The long fire-resistant time provided enough time for people to escape. Therefore, present flame retardant AA coating showed great potential for fire safety of wood structures in buildings in the future.

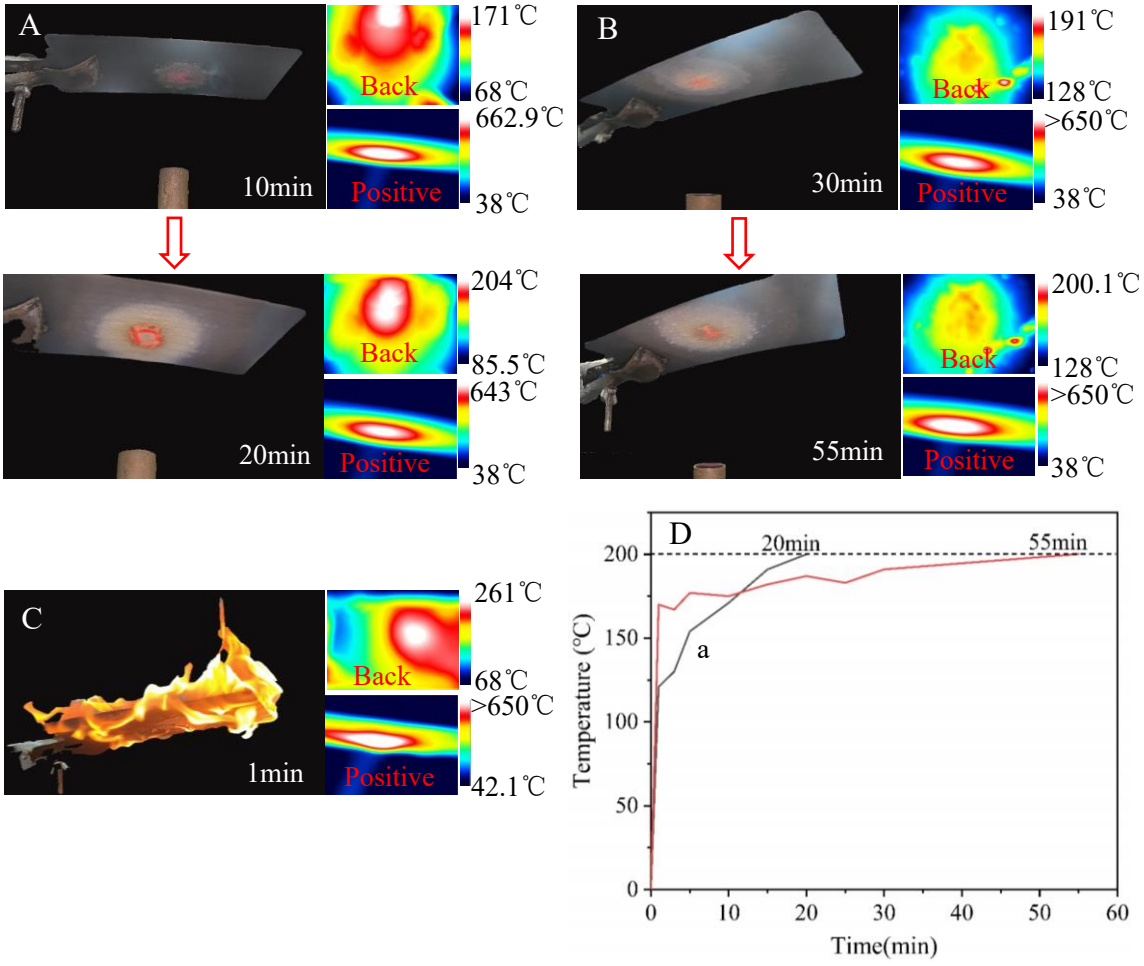

Fig.8. Optical photos of steel plate with (A) GPs@GNs/AA coating, (B) GPs@GNs@PVH/AA coating and (C) AA coating for the burning behavior . (D) Back side temperature of steel plate with (a) GPs@GNs/AA coating and (b) GPs@GNs@PVH/AA coating as a function of times under a flame.

Fig.9 shows the SEM images of various coatings on PMMA substrate after burning. It clearly exhibited porous and loose char layer, which was composed of particles (Fig.9A-B). These discontinuous particles were assigned to residual carbon of AA matrix and inorganic fillers in coating. In a comparison, it showed compact char, in which few particles was observed (Fig.9C). The compact structure was due to that the GPs could melt, flow and fill in these crack and pores of residual carbon in the burning process. Above conclusion was confirmed by heating GPs as shown in sFig.5. When the temperature was higher than 550.0℃, the GPs and GPs@GNs@PVH formed continuous layer with compact structure, while they were difficult to form compact layer at lower temperature than 450.0℃. The elemental mapping images of GPs@GNs@PVH/AA coating after burning was also characterized as shown in Fig.9D. The Si, Na, C and O elements were clearly observed. The C element was assigned to residual carbon of AA matrix and graphene. The Na and O element was assigned to residue of PVH. The Na, Si and O element was also assigned to GPs. These elements were uniformly distributed on surface of char layer. These results further confirmed the formation of uniform and compact char layer. As discussed above, the integral char layer with an compact structure was beneficial for preventing the spread of fire. These results confirmed the lava-like flame retardant mechanism of present GPs@GNs@PVH.

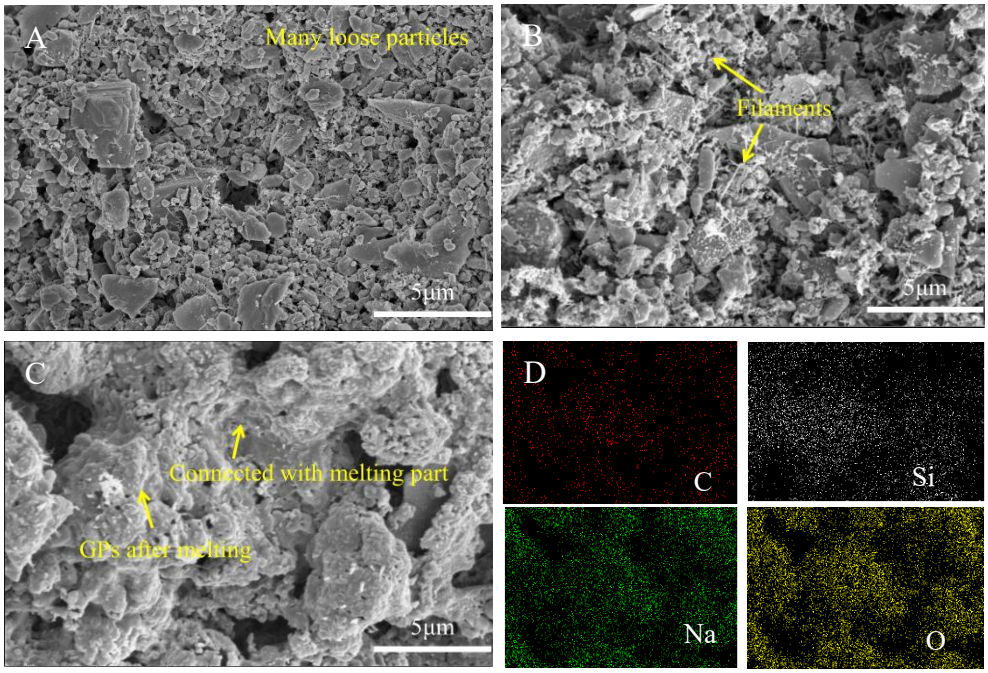

Fig.9. SEM images of (A) AA coating, (B) GPs@GNs/AA coating, (C) GPs@GNs@PVH/AA coating. (D) Elemental mapping image of GPs@GNs@PVH/AA coating.

The melt transition behavior of GPs was further characterized by image burning point tester as shown in Fig.10. It could be seen that the ambient temperature of the test chamber was about 350.0℃, and the middle sample square presents a black image because of the low surface temperature (Fig.10A). The matching program of the test instrument would draw the whole experimental cavity and sample wheel frame with red lines through calculation. After the experiment, when the temperature reached 500.0℃, we could see that the sample suddenly deviated from the area outlined by the red line and contracted to the middle (Fig.10B). This was because the sample began to melt inside and the whole sample collapsed. This was the beginning of the phase transition of the low melting point glass powder. The temperature of phase transition was defined as the collapse temperature. As the temperature continued to 550.0℃, the profile of the sample became a semicircle, indicating that the melting of the sample became more intense. At this time, the temperature was defined as the semicircle temperature. When the temperature reached 590.0℃, the upper part of the sample contour was more and more far away from the original red wheel frame line, and both ends began to spread out beyond the red contour in the initial state. It meant that the low melting point glass powder began to flow under a certain amount of molten state accumulated at this moment. The temperature was defined as the flow temperature. From above discussion, we could further confirm that the phase transition temperature of low melting point glass powder was in the range of 500~590℃.

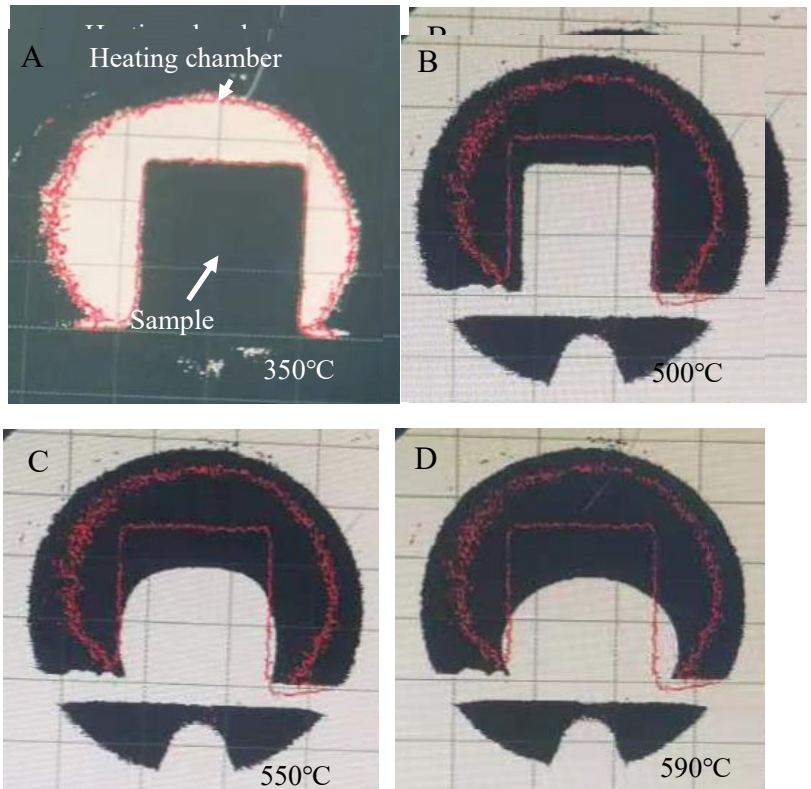

Fig.10. Optical photos of GPs in the test chamber with various temperatures, (A)350℃, (A)500℃, (A)550℃ and (A)590℃ .

The thermal degradation process of GPs@GNs@PVH/AA coating was further investigated by TG-IR spectra as shown in Fig.11. some absorption peaks of 2356.0cm^{-1}, 2067.0cm^{-1}, 1516.0cm^{-1}, 1369~1138.0cm^{-1}, 1755cm^{-1} and 675cm^{-1} were observed, which were assigned to these pyrolysis products of CO_2, CO, CS_2, SO_2, carbonyl and vinylhydrocarbon compounds, respectively[52]. As well-known, GPs and graphene were both thermostable and noncombustible. So, these pyrolysis products were assigned to these organic materials of AA and PVH. These results suggested that the PVH could release some noncombustible gases (e.g., SO_2, CO_2, H_2O), inhibiting the combustion. However, their very weak peaks indicated a low content of these noncombustible gases. The result confirmed that the gas phase mechanism was slight role for good flame retardancy of GPs@GNs@PVH/AA coating.

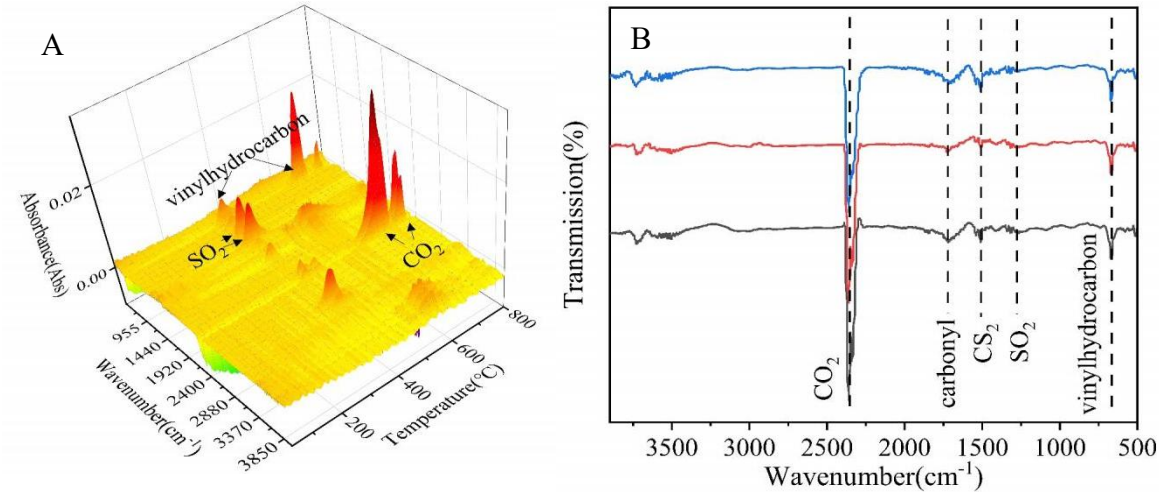

Fig.11. (A)TG-IR 3D image and (B) IR spectra of GPs@GNs@PVH/AA coating as a function of temperatures.

Based on above analysis, a flame retardant mechanism of GPs@GNs@PVH/AA coating was proposed as shown in Fig.12. When the coating was exposure to flame, the AA and PVH polymer began to degrade and gradually created residues. It was accompanied by the release of small volatile gas products, such as CO_2, CO, CS_2, SO_2[53]. Among these gas products, CO_2 and SO_2 were noncombustible gases, which

could inhibit the flame by diluting fuels and oxygen[54]. Moreover, when the GPs@GNs@PVH/AA coating was burnt, the temperature of coating was generally higher than 550.0℃ (Fig.8). With the temperature increasing above 550℃, the GPs began to gradually melt and nearly melted completely at 650℃（sFig.5）. The fully molten GPs could flow freely and thus gradually fill the cracks, forming compact ceramic char layer[46]. Meanwhile, 2D GNs could fill the residual cracks to further improve the structural integrity of the char layer. The compact ceramic char layer does not only prevent the spread of fire and O_2, but also reduce thermal transfer between the flame and the condensed zones. As a result, when the underlying polymer substrates fail to produce enough fuels to feed the flame, the flame could self-extinguish instantly[55].

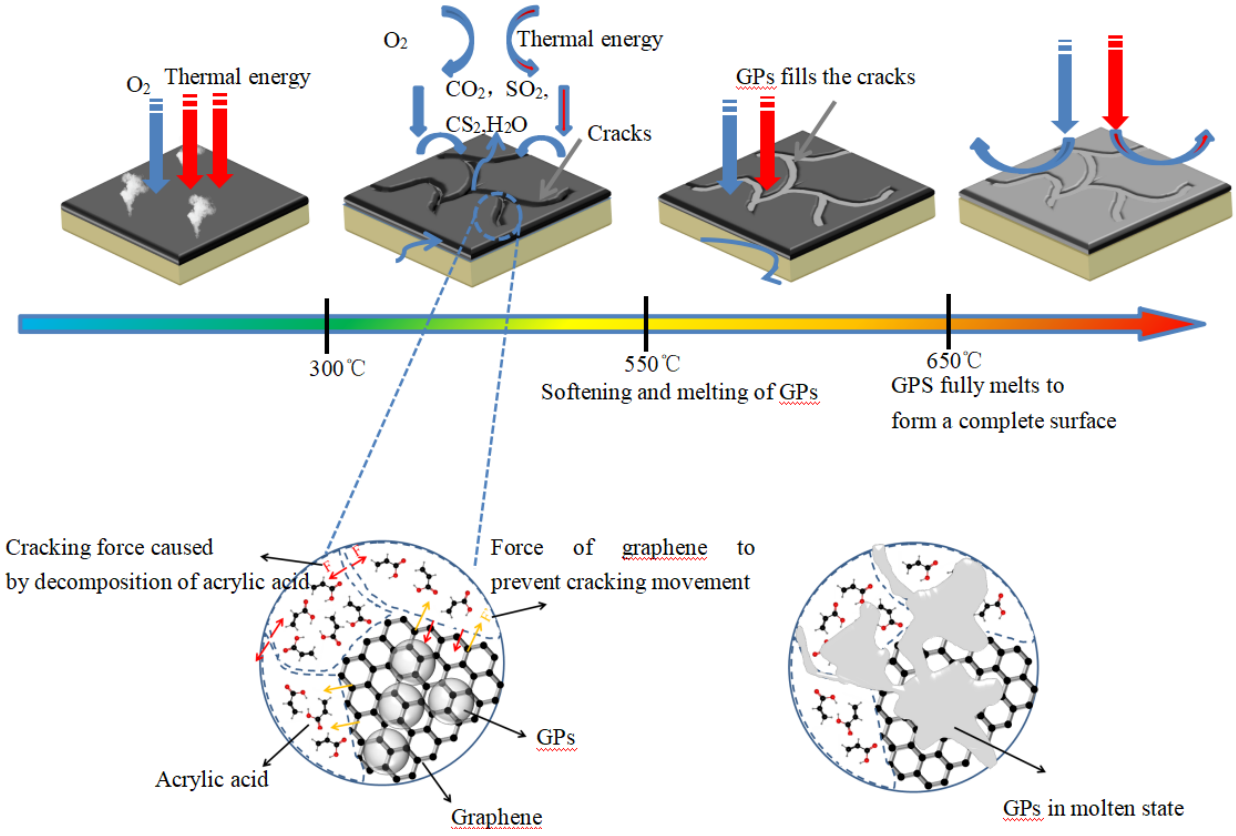

Fig.12. Schemical diagram of fire-retardant mechanism for the GPs@GNs@PVH/AA coating.

4.Conclusion

In summary, a new organic-inorganic hybrid flame retardant was developed by combining with GPs, GNs and PVH for application in flame retardant polymer coating. When the wood was protected by only a 65-um-thick flame retardant AA coating, it

exhibited an ability to self-extinguish, a high LOI of 32.3vol%, a desired UL-94 V-0 rating. Additionally, present flame retardant AA coating also exhibited satisfactory fire/thermal protection for steel, in which the fire-retardant time (55.0min) was obtained at 650-um-thick flame retardant AA coating.This good flame retardancy of GPs@GNs@PVH/AA coating was attributed to formation of noncombustible gases and compact ceramic char layer, resulting from the synergistic effect of GPs, GNs, and PVH. This work opens up a promising avenue for the design of flame retardant thin coatings for diverse real-world applications in the areas of building and construction, transportation, plumbing, and electrics.

Acknowledgments

Financial support from Shanxi Provincial Natural Science Foundation (202104021301059, 201803D421081, YDZJSX2021A026), special fund for science and technology innovation teams of Shanxi province and National Natural Science Foundation of China (U1810114).

Author contributions

Kangtai Ou contributed to investigation, data curation, validation and writing-original draft. Jiang Fan helped with investigation, data curation, and validation. Qingxiao Liu contributed to resources, Qiang Fu contributed to writing-review and editing, Yang Cao contributed to writing-original draft and supervision. Hengyu Zheng helped with conceptualization and writing-original draft. Youyi Sun contributed to project administration,writing-review and funding acquisition.

Ethical statement

This work did not include animal or human subjects and compliance with ethical standards.

Conflict of interest

The authors declare that they have no known competing financial interests or personal relationships that could have appeared to influence the work reported in this paper.

References

[1]X.Q.Qiu, Z.W.Li, X.H.Li, Z.J.Zhang, Flame retardant coatings prepared using layer by layer assembly: A review, Chem. Eng. J. 334(2018)108-122.

[2]Zhewen Ma , Jianzhong Zhang, Lei Liu, Hua Zheng, Jinfeng Dai, Long-Cheng Tang, Pingan Song，A highly fire-retardant rigid polyurethane foam capable of fire-warning，Compos Communi.29(2022)101046.

[3]Haitang Yang , Bin Yu , Pingan Song , Cristian Maluk, Hao Wang, Surface-coating engineering for flame retardant flexible polyurethane foams: A critical review, Compos. Part B: Eng. 176(2019)107185.

[4]B.Sang, Z.W.Li, X.H.Li, L.G.Yu, Z.J.Zhang, Graphene-based flame retardants: a review. J Mater Sci. 51(2016)8271.

[5]Kun-Yu Guo , Qian Wu, Min Mao, Heng Chen, Guo-Dong Zhang , Li Zhao, Jie-Feng Gao , Pingan Song, Long-Cheng Tang, Water-based hybrid coatings toward mechanically flexible, super-hydrophobic and flame-retardant polyurethane foam nanocomposites with high-efficiency and reliable fire alarm response, Compos. Part B: Eng. 193(2020) 108017.

[6]S.Jiang, C.Ji, D.Zha,Y.H.Ding, D.Wu, Q.Yu, Surface Modification of Carbon Microspheres with Guanidine Phosphate and Its Application as a Flame Retardant in PET, Polymers (Basel). 12(2020)1689.

[7]X.Wang, Y.T.Pan, J.T.Wan, D.Y.Wang, An eco-friendly way to fire retardant flexible polyurethane foam: layer-by-layer assembly of fully bio-based substances, RSC Advances. 4(2014)46164.

[8]Fawad Khan, Shanchi Wang, Zhewen Ma, Adnan Ahmed, Pingan Song, Zhiguang Xu, Riping Liu, Huanjie Chi, Jiayi Gu, Long-Cheng Tang, and Yan Zhao, A Durable, Flexible, Large-Area, Flame-Retardant, Early Fire Warning Sensor with Built-In Patterned Electrodes, Small Methods. 5(2021) 2001040.

[9]Chengwei Liu, Tao Zhang, Yuxin Luo, Yixuan Wang, Jiacheng Li , Ting Ye, Ruifeng Guo , Pingan Song, Jiu Zhou, Hao Wang, Multifunctional polyurethane sponge coatings with excellent flame retardant, antibacterial, compressible, and recyclable properties, Compos. Part B: Eng.215(2021)108785.

[10]X.D.Qian, S.H.Jiang, Modification of graphene with organic/inorganic silicon-based materials and its reinforcement on the UV-curing polyurethane composite coatings, Polym. Compos. 39(2018)746.

[11]S.X.Wang, H.B.Zhao, W.H.Rao, S.C.Huang, T.Wang, W.Liao, Y.Z.Wang, Inherently flame-retardant rigid polyurethane foams with excellent thermal insulation and mechanical properties, Polymer. 153(2018)616.

[12]K.Miedzinska, S.Czionka, A.Strakowska, K.Strzelec, Vermiculite Filler Modified with Casein, Chitosan, and Potato Protein as a Flame Retardant for Polyurethane Foams, Int. J. Mol. Sci. 22(2021)10825.
[13]J.Jing,Y.Zhang, Z.P.Fang, D.Y.Wang, Core-shell flame retardant/graphene oxide hybrid:a self-assembly strategy towards reducing fire hazard and improving toughness of polylactic acid, Compos. Sci. Technol. 165(2018)161.
[14]B.Zhao, T.J. Kolibaba, S.Lazar, J.C.Grunlan, Environmentally-benign, water-based covalent polymer network for flame retardant cotton, Cellulose. 28(2021)5855.
[15]T.F.Zhang, C.F.Wang, Yu.Wang, Y.L.Wang, Z.D.Han, Effects of Modified Layered Double Hydroxides on the Thermal Degradation and Combustion Behaviors of Intumescent Flame Retardant Polyethylene Nanocomposites, Polymers (Basel).14(2022)1616.
[16]W.N.Du, Y.Jin, S.Q.Lai, L.J.Shi, Y.C.Shen, J.Z.Pan, Urethane-silica functionalized graphene oxide for enhancing mechanical property and fire safety of waterborne polyurethane composites, Appl. Surf. Sci. 492(2019) 298.
[17]S.M.Kabeb, A.Hassan, .Ahmad, Z.Mohamad, Z.Sharer, M.Mokhtar, Synergistic effects of hybrid nanofillers on graphene oxide reinforced epoxy coating on corrosion resistance and fire retardancy, J. Appl. Polym. Sci.139(2021)51640.
[18]N.Wang, H.W.Teng, F.Yang, J.Q.You, J.Zhang, D.Y.Wang, Synthesis of K-Carrageenan Flame-Retardant Microspheres and Its Application for Waterborne Epoxy Resin with Functionalized Graphene, Polymers. 11(2019)1708.
[19]X.X.Chen, J.F.Li, M.Gao, L.N.Yue, X.Zhou, Fire Protection Properties Of Wood In Waterborne Epoxy Coatings Containing Functionalized Graphene Oxide, J. Wood Chem. Technol. 39(2019) 313.
[20]Ting Sai, Shiya Ran, Zhenghong Guo, Pingan Song, Zhengping Fang, Recent advances in fire-retardant carbon-based polymeric nanocomposites through fighting free radicals, SusMat.2(2022) 411.
[21]Lei Liu, Jiabing Feng, Yijiao Xue, Venkata Chevali, Yubai Zhang, Yongqian Shi, Long-Cheng Tang, Pingan Song, 2D MXenes for Fire Retardancy and Fire-Warning Applications: Promises and Prospects, Adv. Funct. Mater.33(2022) 2212124.
[22]X.D.Qian, L. Song, B.Yu, B.B.Wang, B.H.Yuan, Y.Q. Shi, Y.Hu, R.K.K.Yuen, Novel organic–inorganic flame retardants containing exfoliated graphene: preparation and their performance on the flame retardancy of epoxy resins, J. Mater. Chem. A. 1(2013)6822-6830.

[23]S.Liu, Z.P.Fang, H.Q.Yan, V.S. Chevali, H.Wang, Synergistic flame retardancy effect of graphene nanosheets and traditional retardants on epoxy resin, Composites: Part A. 89 (2016)26-32.

[24]Qiang Chen, Lei Liu, Anlin Zhang , Wenduo Wang , Zhengzhou Wang, Jianzhong Zhang, Jiabing Feng, Siqi Huo, Xuesen Zeng , Pingan Song, An iron phenylphosphinate@graphene oxide nanohybrid enabled flame-retardant, mechanically reinforced, and thermally conductive epoxy nanocomposites, Chem. Eng. J. 454(2023)140424.

[25]R.Duan, Ho.J.Wu, J.H.Li, Z.X.Zhou, W.H.Meng, L.Liu, H.Q.Qu, J.Z.Xu, Phosphor nitrile functionalized UiO-66-NH2/graphene hybrid flame retardants for fire safety of epoxy, Colloids and Surfaces A: Physicochemical and Engineering Aspects. 635(2022)128093.

[26] X.L.Yu, B.B.Wang, P.F.Jia, Z.T.Yin, G.Tang, X.D.Zhou, T.T.Lu, L.Y.Guo, L.Song, Y.Hu, Effects of graphene nanosheets decorated by cerium stannate on the enhancement of flame retardancy and mechanical performances of flexible polyurethane foam composites, Polym. Adv. Technol. 33(2022)290-302.

[27]X.W.Han, S.Guo, H.Y.Pan, Construction of $Mg(OH)_2$/graphene oxide nanostructures with advanced adsorbing and flame-retardancy performance, Mater. Chem. Phys. 290 (2022)126653.

[28]H.D.Lu, L.Song, Y.Hu, A review on flame retardant technology in China. Part II: flame retardant polymeric nanocomposites and coatings, Polym. Adv. Technol. 22(2011)379-394.

[29]C.Chi, M.Ma, H.Tai, C.L.Chiang, H.C.Kuan, J.C.Yang, C.W.Hsu, Preparation and Properties of Toughened Novolac Type Phenolic/SiO_2 Flame Retardant Nanocomposite, Compos Technol. 2020(2004)742-747.

[30]Z.W.Ma, X.C.Liu, X.D.Xu, L.Liu, B.Yu, C.Maluk, G.B.Huang, H.Wang, P.G. Song, Bioinspired, Highly Adhesive, Nanostructured Polymeric Coatings for Superhydrophobic Fire-Extinguishing Thermal Insulation Foam, ACS NANO. 15(2021)11667.

[31]N.F.Attia, S.E.A.Elashery, A.M.Zakria, A.S.Eltaweil, H.Oh, Recent advances in graphene sheets as new generation of flame retardant materials, Mater. Sci. Eng:B. 74(2021)115460.

[32]Z.Q.Li, W.Li, L.Liao, J.B.Li, T.Wu, L.C.Ran, T.B.Zhao, B.S.Chen, Preparation and properties of polybutylene-terephthalate/graphene oxide in situ flame-retardant material, J. Appl. Polym. Sci. 137(2020) 49214.
[33]H.L.Xie, X.JLai, H.Q.Li, J.F.Gao, X.R.Zeng, X.Y.Huang, S.F.Zhang, A sandwich-like flame retardant nanocoating for supersensitive fire-warning, Chem. Eng. J. 382(2020)1385.
[34]G.Huang, C.C.Lv, J.X.He, X.Zhang, C.Zhou, P.Yang, Y.Tan, H.Huang, Study on Preparation and Characterization of Graphene Based on Ball Milling Method, J. Nanomater. 2020(2020)1.
[35]K.Hatakeyama, Y.Hakuta, J.Sugiyama,Y.Shimizu, A simple ozone bubbling procedure for the preparation of graphene oxide. Jpn. J. Appl. Phys. 58(2019)5.
[36]N.X.Liu, Q.G.Tang, B.Huang, Y.P.Wang, Graphene Synthesis: Method, Exfoliation Mechanism and Large-Scale Production, Crystals. 12(2021)25.
[37]S.P.Zhang, X.D.Yang, Z.B.Tu, W.D.Hua, P.H.He, H.H.Li, B.Zhang, T.R.Ren, Influence of the hydrophilic moiety of polymeric surfactant on their surface activity and physical stability of pesticide suspension concentrate, J. Mol. Liq. 317(2020)114136.
[38]M.E. Moustapha, J.F. Friedrich, Z.R. Farag, S.Krüger, M.Farouk, Plasma deposition of adhesion-promoting polymer layers onto polypropylene for subsequent covering with thick fire retardant coatings, J. Adhes. Sci. Technol. 29(2015) 1522-1533.
[39]M.A. Bhakare, K.D. Lokhande, M.P. Bondarde, P.S. Dhumal, S.Some, Dual functions of bioinspired, water-based, reusable composite as a highly efficient flame retardant and strong adhesive, Chem. Eng. J. 454 (2023)140421.
[40]S.T.Yang, C.Liu, Z.K.Sun, M.Q.Xu, Y.D.Feng, Effects of resin pre-coating treatment and fibre reinforcement on adhesive bonding between CFRP sheet and concrete. Compos. Struct. 292(2022)115610.
[41]N.K. Fukumasu, R.M.Souza, Numerical evaluation of cohesive and adhesive failure modes during the indentation of coated systems with compliant substrates, Surf coat Tech. 260 (2014)266-271.
[42]J.V. Nardeli, C.S. Fugivara, M.Taryba, M.F. Montemor, S.J.L.Ribeiro, A.V. Benedetti, Novel healing coatings based on natural-derived polyurethane modified with tannins for corrosion protection of AA2024-T3, Corros. Sci. 162(2020)108213.

[43]Y.Y.Huan, G.L.Wang, C.Q.Li, G.F.Li, Acrylic acid grafted-multi-walled carbon nanotubes and their high-efficiency adsorption of methylene blue, J. Mater. Sci. 55(2020) 4656.
[44]Yanchao Shi, Guojian Wang, The novel epoxy/PEPA phosphate flame retardants: Synthesis, characterization and application in transparent intumescent fire resistant coatings, Prog. Org. Coat.. 97 (2016) 1–9.
[45]A.Hejna, Clays as Inhibitors of Polyurethane Foams' Flammability. Materials (Basel).14(2021)4826.
[46]Ma ZW,Zhang JZ ,Maluk C, Yu YM , Seraji SM,Yu B ,Wang H,Song PA, A lava-inspired micro/nano-structured ceramifiable organic-inorganic hybrid fire-extinguishing coating,Matter.5(2022)911~932.

[47]S.Li, X.H.Wang, M.J.Xu, L.N.Liu, W.B.Wang, S.L.Gao, B.Li, Effect of a biomass based waterborne fire retardant coating on the flame retardancy for wood, Polym. Adv. Technol. 32(2021)1-10.
[48]L.M.Chen, S.H.Zeng, Y.Xu, W.Y.Nie, Yi.F.Zhou, P.P.Chen, Epoxy-modified silicone resin based N/P/Si synergistic flame-retardant coating for wood surface, Prog. Org. Coat. 170(2022)106953.
[49]D.Naik, K.Wazarkar, A.Sabnis, UV-curable flame-retardant coatings based on phosphorous and silicon containing oligomers, J. Coat. Technol. Res. 16(2019)733-743.
[50]Y.H.Huang, T.T.Ma, L.P.Li, Q.W.Wang, C.G.Guo, Facile synthesis and construction of renewable, waterborne and flame-retardant UV-curable coatings in wood surface, Prog. Org. Coat. 172(2022)107104.
[51]M.L.Li, X.H.Hao, M.L.Hu, Y.H.Huang, C.Tang, Y.Y.Chen, L.P.Li, Synthesis of vanillin-based flame retardant epoxy coating on wood surface, Prog. Org. Coat. 172 (2022)107161.
[52]B.Zhao, T.J.Kolibaba, S.Lazar, J.C. Grunlan, Environmentally-benign, water-based covalent polymer network for flame retardant cotton, Cellulose. 28(2021) 5855-5866.
[53]B.Tawiaha, B.Yu, R.C.Wei, R.K.K. Yuen, W.Chen, J.H.Xin, B.Fei, Simultaneous fire safety enhancement and mechanical reinforcement of poly (lactic acid) biocomposites with hexaphenyl (nitrilotris(ethane-2,1-diyl))tris (phosphoramidate), J. Hazard. Mater. 380(2019)120856.

[54]B.Tawiah, Y.Y.Zhou, R.K.K.Yuen, J.Sun, B.Fei, Microporous boron based intumescent macrocycle flame retardant for poly (lactic acid) with excellent UV protection, Chem. Eng. J. 402(2020)126209.
[55]Y.Y.Zhou, B.Tawiah, N.Noor, Z.Zhang, J.Sun, R.K. K. Yuen, B.Fei, A facile and sustainable approach for simultaneously flame retarded, UV protective and reinforced poly(lactic acid) composites using fully bio-based complexing couples, Compos Part B-ENG. 215(2021)108833.